COMPARATIVE EVALUATION OF ICING ON AERODYNAMIC SURFACES

D. Raps*, S. Jung*, T. Strobl*
***EADS Innovation Works, Metallic Technologies & Surface Engineering,**
81663 Munich, Germany

Dominik.Raps@eads.com;Tobias.Strobl@eads.com

Abstract

In this study, the formation and adhesion of ice to solid substrates with different surface properties is compared. It provides an overview of icing test methods to analyze the freezing delay, droplet impact, runback icing and ice adhesion on aerodynamic surfaces.

The investigations have shown the feasiblity of a smooth hydrophobic and nano-textured super hydrophobic coating configuration to fulfill a passive ice resistance on aerodynamic surfaces. For achieving anti-icing properties at the impact area of supercooled water droplets (e.g. leading edge), smooth coatings with low surface free energy (e.g. hydrophobicity) achieved by an appropriate chemical composition seem to be the most promising approach. In contrast super hydrophobic coatings with low water contact angle hysteresis performed best to carry the accumulated water within the aerodynamic boundary layer away from the body-surface. The affinity for ice adhesion is significantly influenced by the water contact angle of the respective sample.

1 General Introduction

The development of future aircrafts is driven substantially by decreasing fuel consumption and CO_2 emission. One challenge for surfaces is the desired property of ice resistance. This presentation provides an overview of icing test methods to analyze the freezing delay, droplet impact, runback icing and ice adhesion on aerodynamic surfaces.

A number of laboratory experiments were conducted in the past to study the adhesive properties of ice on solid surfaces [1 - 4]. Within the experimental procedure, the ice is considered as polycrystalline ice Ih, which generally is formed when liquid water is cooled down below zero degrees Celsius (°C) at standard atmospheric pressure (1.01325 bar) [5]. The density ρ of ice Ih at 0 °C is equal to 0.91671 ± 0.00005 g/cm³ and the Young's modulus of ice roughly amounts to 9.0 GPa [6, 7]. In addition, the Poisson ratio of isotropic polycrystalline ice was determined as to be 0.325 [8]. Table I. summarizes the main physical parameters for polycrystalline ice Ih.

TABLE I. MAIN PARAMETERS FOR POLYCRYSTALLINE ICE I_h

Parameter	*Value*
Density ρ	0.91671 ± 0.00005 g/cm³
Young's modulus E	9.0 GPa
Poisson ratio ν	0.325

2 Experimental

2.1 Freezing delay

The test device features mono-disperse super-cooled water droplets that are generated by a piezo-electric jetting device and introduced into the cooled chamber through a copper tube. The control section was cooled by means of a cold gas generator. The water droplet/coating interaction such as droplet impact, accumulation and crystallization was monitored using a high speed camera. Droplet impact and accumulation were tested at – 20 °C using a droplet diameter of 60 µm and an angle of attack of 90°. Fig. 1 shows a schematic drawing of the test setup.

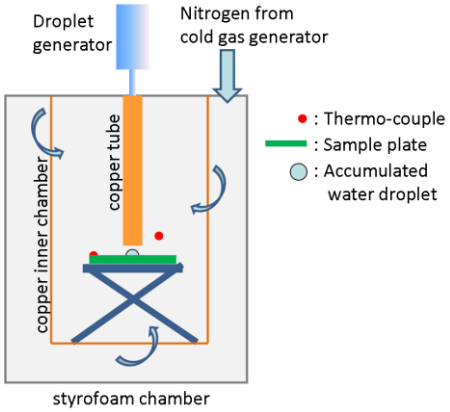

Fig. 1: Cooled Water Droplet Tunnel Box Setup.

2.2 Runback Icing

The runback icing tests are performed using the cooling chamber in Fig.1 with an integrated wind tunnel (cross test section: 5 cm x 5 cm, max. free stream velocity: 10 m/s). A 5 µL water droplet was placed on a flat horizontal test sample, positioned into the middle of the test section. The free stream velocity of the gaseous nitrogen was gradually increased until the droplet starts freezing or to roll/drift off the test sample surface downstream. The temperatures of the water droplet, the sample surface and the gaseous nitrogen kept constant within -16 °C ± 0.5 °C for the whole experiment.

2.3 Supercooled water droplet impact

A cryogenic closed wind tunnel (cross test section: 10 cm x 15 cm, max. free stream velocity: Mach 0.35) was used to study the impact behaviour of supercooled water droplets on a scaled NACA0024 profile leading edge. Water droplets (~60 µm dia.) were generated and injected into the nitrogen gas stream through a vertical outer-profile-inner-tube configuration upstream of the contraction section of the tunnel. The temperature of the injected water droplets deceased from room temperature to free stream temperature within the inner tube before getting carried away and accelerated to free stream velocity by the nitrogen gas. The supercooled water droplets then impacted within an area of 1 cm x 1 cm onto the leading edge of the scaled NACA0024 profile (angle of attack: 0°). The temperature of the nitrogen gas, the water droplets and the test sample was monitored continuously and kept constant during the measurement. Fig. 2 gives an overview of the wind tunnel design and the drop delivery concept.

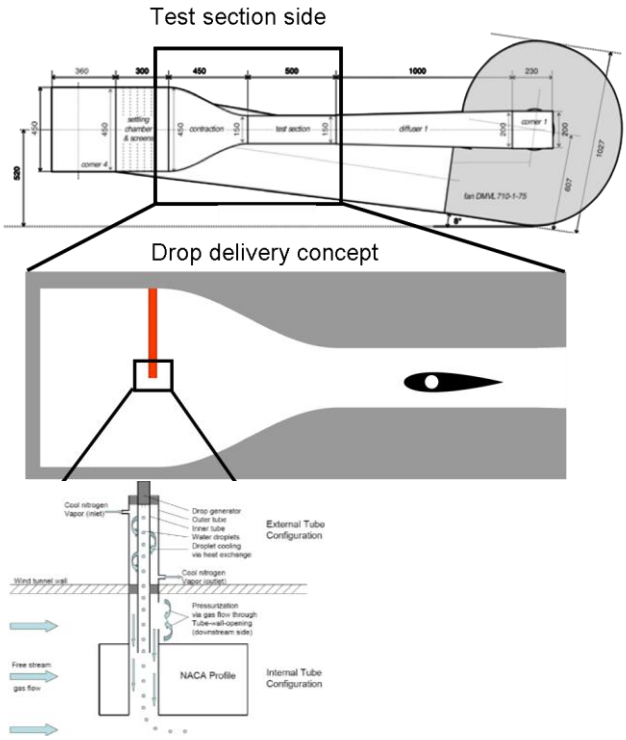

Fig. 2: Cryogenic Wind Tunnel Configuration.

2.4 Ice adhesion

Subsequent to the ice accretion process, each ice-substrate composite beam is centrically clamped onto an electro-magnetic shaker. Each ice-substrate composite beam is vibrated by means of the electro-magnetic shaker submitting a sinusoidal stimulus to the sample. Since the ice layer is not continuously accreted on the substrate surface over the entire length and due to the damping effect of the strain gauge as well, the first resonance frequency of the ice-substrate composite beam is approached through the determination of the first resonance frequency of the bare aluminum beam without ice coating and strain gauge. The first resonance frequency of the aluminum beam without ice coating is equal to approximately 254.0 Hz. The excitation amplitude of the shaker is then increased until the resultant interfacial shear stress leads to ice de-bonding from the substrate

surface, i.e. adhesive failure occurs in the interface between the ice and the metal substrate.

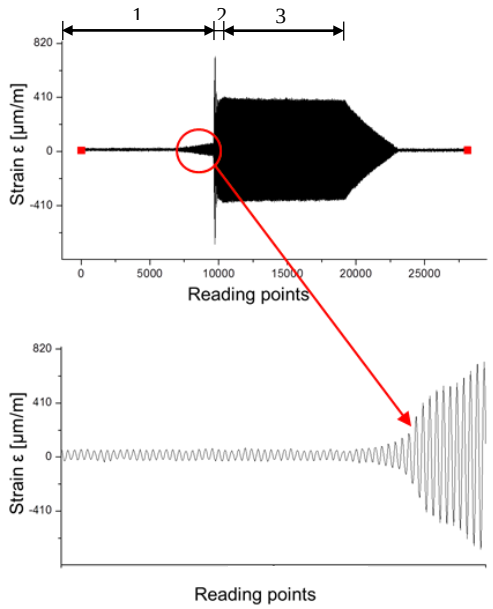

Fig. 3: Strain gauge reading of an ice-substrate composite beam

By means of the strain gauge reading, the adhesive failure can be detected as the bending stiffness of the composite beam changes due to ice breakage and subsequent delamination from the beam surface. Figure 3 illustrates an exemplary strain gauge reading of an ice-substrate composite beam under harmonic excitation, where 500 reading points are recorded every second.

The delamination process of the ice from the sample can be subdivided into three phases. The first phase is characterized by a continuous increase in the oscillation amplitude, ending with a sudden peak in the vertical axis of the vibration pattern. This is the point where the ice starts to de-bond from the substrate surface. As visually observed, the ice starts to delaminate close to the clamping of the composite beam due to the fact that within this area, the maximum bending moment along the x-axis is obtained. After the initiation of ice delamination, the amplitude is not increased further. The second phase of the waveform of the oscillatory motion is characterized by a maximum in the oscillation amplitude, which is caused by the instantaneous decrease in the bending stiffness of the beam due to the ice delamination. Hence, the damping effect of the ice on the vibrational motion is reduced and the oscillatory motion requires a certain time to settle down at a stable level. Since the excitation amplitude is constant in the ensuing period, the third phase shows constant values for the strain of the beam. For the determination of the maximum adhesion strength of ice onto solid surfaces, the corresponding reading of the strain gauge is considered on the verge of the sudden peak at the end of phase one, where the ice layer is still entirely bonded to the metal substrate. This value of the strain εEF_al is substituted into equation (3) to compute the maximum admissible shear stress τint at the interface between the ice and the aluminum beam just before the ice detaches.

2.5 Examined Coatings

Table 1. Coating types for freezing delay and runback ice studies

No.	Coating type
1	Hydrophobic sol-gel coating
2	Epoxy coat. bearing freezing point depressants
3	Polyurethane clear coat
4	Super hydrophobic fluoro-silane coating (TiO_2 nanotube based)
5	Super hydrophobic coating (PTFE-particle based)

Table 2. Coating types for ice adhesion measurements

No.	Coating type
1	AA2024 anodized
2	AA2024 reference
3	Hard anodized Aluminium with Teflon particles
4	Hydrophobic polyurethane topcoat

3 Results and Discussion

3.1 Freezing Delay

Inkjet deposit droplets landed within an area of 300 - 500 µm across and coalesced into a single growing droplet before freezing. Fig. 4 (exemplify graph) shows median values of the time until freezing on each surface, based on a minimum of 12 data points per sample plate. A comparison of the median values showed correlations between surface roughness and water contact angle (see Fig. 4). Very smooth surfaces performed the best whereas for rougher surfaces (super hydrophobic surfaces) the freezing resistance was dominated by water contact angle only.

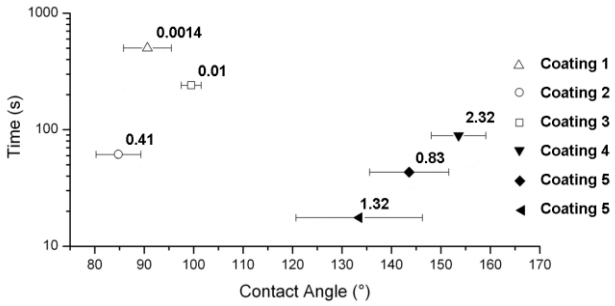

Fig. 4: Time to freezing vs. Contact Angle

(Values beside each symbol: Surface roughness).

3.2 Runback Icing

The study of the roll-off/drift behavior of 5 µL supercooled water droplets on flat surfaces under forced confection reveal the advantage of superhydrophobic surfaces with low water contact angle hysteresis in terms of low adhesion and wettability: In all cases where the droplets overcame the adhesive forces and started to roll off because of the applied aerodynamic forces, no crystallization took place for the entire roll-off distance. This behaviour was independent of the difference of hydrophobic textures tested in this experiment. Smooth surfaces with contact angles close to 90° started moving at much higher gas velocities compared to all superhydrophobic textures and crystallized during slipping motion. The nucleation stared invariably on the gas-water interphase upstream the droplet which is due to the highest extraneous cause of forced confection in that area.

3.3 Supercooled water droplet impact

The impact of free falling supercooled water droplets on flat sample surfaces was compared with those carried in a cooled free stream nitrogen gas flow impacting on a scaled NACA0024 profile leading edge. Supercooled 60 µm-dia. droplets (-20 °C) bounced off instead of accumulating on super hydrophobic surfaces (Fig. 5B). Larger droplets within the range of 5 µL froze instantaneously by touching the surface and kept their impact location (Fig. 5A). The present results indicate a direct correlation between deformation, temperature, and nucleation probability of an impinging supercooled water droplet.

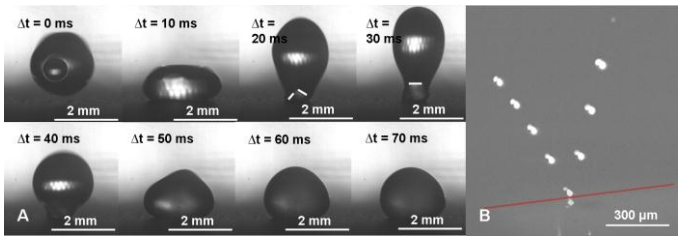

Fig. 5: Supercooled water droplet – super hydrophobic surface interaction. (A) Impact of a 5 µL droplet with crystallization initiation at the water – substrate interface. The white lines in sequence 3 and 4 mark the instantaneous position of the freezing front. (B) Bouncing of a 60 µm-dia. droplet without crystallization. The red line indicates the water droplet – substrate interface (High-speed imaging sequence: 2 ms).

3.4 Ice Adhesion

Fig. 6 shows the mean values of the maximum interfacial shear stress τint plotted against the water contact angle θ of the respective substrate surface. The lowest value of interfacial shear stress is obtained for the hydrophobic polyurethane coating with a magnitude of 0.025 ± 0.008 MPa. The reason for the very low adhesion of ice to this coating is based upon the large contact angle with water. This means that solely a small part of each individual water droplet is in intimate contact with the substrate surface and respectively freezes onto it. The

measurement results also indicate that the presence of embedded Teflon (PTFE) particles in the hard anodizing layer leads to a rather low value of ice adhesion with a magnitude of 0.044 ± 0.005 MPa. However, since the coating contains Teflon particles to a limited extent, its contact angle with water does not attain typical values for Teflon such as 108° as stated by Ref. [9]. Hence, the efforts to remove the ice from this coating are in excess of those applying to coatings that are entirely made out of Teflon. Comparing the AA 2024 clad reference sample to the previous coatings the adhesion of ice to the former increases up to a magnitude of 0.050 ± 0.005 MPa. This is due to the presence of hydroxyl groups at the substrate surface and the resultant increase in the degree of hydrophility, which is depicted by the decrease in the water contact angle. The anodized AA 2024 sample shows the highest value of ice adhesion to the substrate material in the experiments. In accordance with Ref. [10], reactive groups with available bonding sites such as the OH^- groups on the surface of the anodized sample considerably increase the attraction between the ice and the substrate surface. Thus, the ice adhesion behavior of the anodized AA 2024 specimen is related to the large amount of hydrophilic OH^- groups and also to the open porous aluminum oxide surface structure. Taken together, this leads to a high mean value of the interfacial shear stress τint with a magnitude of 0.072 ± 0.006 MPa.

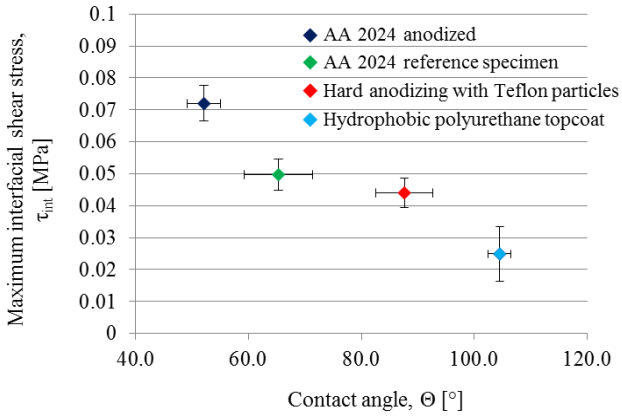

Fig. 6: Relation between the water contact angle θ and the maximum interfacial shear stress τint of the ice-substrate composite beams

4 Conclusion

The current investigation has shown the feasiblity of a smooth hydrophobic and nano-textured super hydrophobic coating configuration to fulfill a passive ice resistance on aerodynamic surfaces. For achieving anti-icing properties at the impact area of supercooled water droplets (e.g. leading edge), smooth coatings with low surface free energy (e.g. hydrophobicity) achieved by an appropriate chemical composition seem to be the most promising approach. In contrast super hydrophobic coatings with low water contact angle hysteresis performed best to carry the accumulated water within the aerodynamic boundary layer away from the body-surface. Another main conclusion is that very high contact angles are good for low ice adhesion properties. In this context, hydrophobic coatings with a contact angle θ greater than 90 ° showed the best performance for low ice adhesion. For future aircraft applications, it will be of great interest to further investigate the optimum surface roughness combined with a very high water contact angle for ease in ice removal.

Acknowledgments

The authors would like to acknowledge the funding provided by the European Community (AEROMUCO project: “AERODynamic Surfaces by advanced MUltifunctional COatings”, Contract N° FP7-AAT-2010-RTD-1- 266029).

References

[1] Akitegetse, C., Volat, C., & Farzaneh, M. (2008). Measuring bending stress on an ice/aluminium composite beam interface using an embedded piezoelectric PVDF (polyvinylidene-fluoride) film sensor. *Meas. Sci. Technol.* (19), 1-9.

[2] Hassan, M. F., Lee, H. P., & Lim, S. P. (2010). The variation of ice adhesion strength with substrate surface roughness. *Meas. Sci. Technol.* (21), 1-9

[3] Javan-Mashmool, M., Volat, C., & Farzaneh, M. (2006). A new method for measuring ice adhesion strength at an ice–substrate interface. *Hydrol. Process.* (20), 645–655.

[4] Archer, P., & Gupta, V. (1998). Measurement and control of ice adhesion to aluminum 6061 alloy. *J. Mech. Phys. Solids* (46), 1745-71.

[5] Hobbs, P. V. (1974). *Ice Physics.* London: Oxford University Press.

[6] Mojtaba, E. (2005). *Ice shedding from overhead electrical lines by mechanical breaking: a ductile model for viscoplastic behaviour of atmospheric ice.* Chicoutimi: Université du Québec.

[7] Ginnings, D. C., & Corruccini, R. J. (1947). An improved ice calorimeter - the determination of its calibration factor and the density of ice at 0°C. *J. Res. natn Bur. Stand* (38), 583-91.

[8] Gammon, P. H., Kiefte, H., Clouter, M. J., & Denner, W. W. (1983). Elastic Constants of Artificial and Natural Ice Samples by Brillouin Spectroscopy. *Journal of Glaciology , 29* (103), 433-60.

[9] Raraty, L. E., & Tabor, D. (1958). The adhesion and strength properties of ice. *Proc. R. Soc.* (A 245), 184-201.

[10] Sivas, S. L., Riegler, B., Thomaier, R., & Hoover, K. (2004). *A Silicone-Based Ice Phobic Coating for Aircraft.* The Department of the Army, Engineer Research and Development Center, Cold Regions Research and Engineering Laboratory (CRREL). Hanover, NH, U.S.: Pratt & Whitney.

Copyright Statement